

RESEARCH

Open Access



# Doxorubicin loaded exosomes inhibit cancer-associated fibroblasts growth: in vitro and in vivo study

Fatemeh Akhavan Attar<sup>1</sup>, Shiva Irani<sup>1\*</sup>, Mana Oloomi<sup>2</sup>, Azam Bolhassani<sup>3</sup>, Loabat Geranpayeh<sup>4</sup> and Fatemeh Atyabi<sup>5</sup>

## Abstract

Cancer-associated fibroblast cells (CAFs) play a key role in the breast cancer (BC) microenvironment that induces resistance to chemotherapy. Adipose mesenchymal stem cells (ADMSCs) derived exosomes were utilized to deliver the doxorubicin (Dox) to BC cell lines (MDA-MB-231, MCF-7) and CAFs in both mono and co-culture systems. Immunocytochemistry (ICC) for VIMENTIN and flow cytometry for the CD45, CD34, CD73, and CD90 markers were used to confirm the phenotypic characteristics of CAFs and MSC cells. Dox was loaded into ADMSCs-derived exosomes (Exo-Dox) through sonication and its loading was confirmed by transmission electron microscope (TEM). Compared to free Dox, Exo-Dox showed a higher efficiency in inducing apoptosis and inhibiting growth and migration in co-culture cells with CAFs ( $P < 0.05$ ). The up-regulation of *H19* and *UCA1* lncRNAs, associated with chemoresistance, was confirmed using real-time PCR in CAF-derived breast cancer patients, CAF-derived exosomes, and exosome-derived patient serums. *H19* and *UCA1* expression levels were significantly down-regulated in MDA-MB-231, MCF-7, and co-cultures of MDA-MB-231 and MCF-7 cells with CAFs that received Exo-Dox treatment. In vivo results indicated that ADMSCs-derived exosomes (MSC-Exos) can accumulate at the tumor site. Exo-Dox suppressed cancer cell growth and significantly decreased tumor size compared to PBS ( $p < 0.01$ ). The findings confirmed the growth inhibition effects of Exo-Dox in CAFs, BC cells, and tumor-bearing mice.

**Keywords** Cancer-associated fibroblast cells, Exosomes, Doxorubicin, Breast cancer, Drug delivery

## Introduction

Breast cancer (BC) is the most prevalent threat and a leading cancer-caused death in women around the world. It still presents a significant health issue due to the high rates of invasion, metastasis, recurrence, and drug resistance [1]. Drug resistance remains a challenge in the treatment of BC despite substantial advancements in the field. A better understanding of the tumor microenvironment and its implications for drug resistance, cancer-associated fibroblasts (CAFs) has identified as significant contributors to the progression of BC and drug resistance. CAFs represent a diverse group of stromal cells activated by cancer cells and capable of secreting various factors that regulate tumor growth. Moreover, CAFs

\*Correspondence:

Shiva Irani  
s.irani@srbiau.ac.ir

<sup>1</sup>Department of Biology, Science and Research Branch, Islamic Azad University, Tehran, Iran

<sup>2</sup>Department of Molecular Biology, Pasteur Institute of Iran, Tehran, Iran

<sup>3</sup>Department of Hepatitis and AIDS, Pasteur Institute of Iran, Tehran, Iran

<sup>4</sup>Department of 4th Surgery, Sina Hospital, Tehran, Iran

<sup>5</sup>Department of Pharmaceutical Nanotechnology, School of Pharmacy, Tehran University of Medical Sciences, Tehran, Iran



© The Author(s) 2025. **Open Access** This article is licensed under a Creative Commons Attribution-NonCommercial-NoDerivatives 4.0 International License, which permits any non-commercial use, sharing, distribution and reproduction in any medium or format, as long as you give appropriate credit to the original author(s) and the source, provide a link to the Creative Commons licence, and indicate if you modified the licensed material. You do not have permission under this licence to share adapted material derived from this article or parts of it. The images or other third party material in this article are included in the article's Creative Commons licence, unless indicated otherwise in a credit line to the material. If material is not included in the article's Creative Commons licence and your intended use is not permitted by statutory regulation or exceeds the permitted use, you will need to obtain permission directly from the copyright holder. To view a copy of this licence, visit <http://creativecommons.org/licenses/by-nc-nd/4.0/>.

contribute to drug resistance by secreting of modulators that reduce the efficacy of chemotherapy and targeted therapies. Consequently, targeting CAFs could be a possible strategy to enhance the effectiveness of BC treatment [2].

Long non-coding RNAs (lncRNAs), which can affect cancer cell proliferation, apoptosis, and metastasis, are also significant regulators of drug resistance in cancer [3].

There is substantial evidence supporting the involvement of lncRNAs and CAFs in mediating drug resistance in cancers. Notably, several studies have indicated that lncRNAs can potentiate CAF activation and the release of pro-tumorigenic molecules. Conversely, other studies have demonstrated that lncRNAs can reduce drug resistance caused by CAFs. Additionally, some research has shown that CAFs contribute to drug resistance through the secretion of exosomes containing lncRNAs [4]. For instance, exosomes secreted by CAFs, which include *H19*, can promote the catenin pathway and chemoresistance in colorectal cancer [5].

Several studies have indicated that *UCA1* induces treatment resistance in BC cells by preventing apoptosis and increasing cell survival. Exosomes carrying the lncRNA *UCA1* derived from CAFs have been reported to increase treatment resistance in vulvar squamous cell carcinoma [6]. Therefore, targeting *H19*, *UCA1*, and their interactions with CAFs may represent a promising approach to overcoming drug resistance in BC.

One of the most crucial chemotherapy treatments employed for both early and advanced stages of BC is Dox, which has limitations such as cardiotoxicity [7, 8]. One approach to overcome these limitations is using nanocarriers to enhance the delivery of Dox to the tumor site while minimizing off-target effects [9, 10].

Small extracellular vesicles, known as exosomes, are released by diverse cell types, such as mesenchymal stem cells (MSCs) and cancer cells [11, 12]. Exosomes exhibit diameters ranging from 40 to 200 nm [13]. Characterized by their small size, stability, and ability to target specific cells and tissues, they are promising candidates for drug delivery to cancer cells [14].

MSCs-derived exosomes (MSC-Exos) also possess immunomodulatory and regenerative properties, which can enhance their therapeutic potential in BC treatment. They may strengthen the immune system, inhibit tumor metastasis, promote tissue regeneration, and suppress tumor growth [15].

Dox can be effectively delivered to BC cells and tumors using MSC-Exos. This method may increase the drug's concentration within the tumor, thereby enhancing its therapeutic efficacy while reducing its cardiotoxicity [16]. Exosomes are also incorporated into the enhanced preclinical development method for Dox (Exo-Dox) [17].

It is hypothesized that the up-regulation of *H19* and *UCA1* by CAFs and CAFs derived exosomes plays a role in the invasion and chemoresistance of BC. This study is an attempt to investigate the efficacy of mesenchymal Exo-Dox in the chemosensitivity of MCF-7, MDA-MB-231 cells, as well as CAFs, in both mono and co-culture systems by down-regulating the *H19* and *UCA1*. The steps of the study are presented in a flowchart as supplementary data (S1).

## Materials & methods

### Samples

Fresh BC tissue and serums were collected from 10 patients with invasive ductal carcinoma (IDC) who did not receive any prior treatments. The surgical procedures were carried out at the Farmaniyeh and Sina hospitals. Additionally, serum samples were collected from 10 healthy female individuals who provided blood samples. Adipose tissue was acquired from a 45-year-old woman who underwent liposuction at Alborz Hospital. A consent letter was signed by all women and the Ethical Committee of the Islamic Azad University approved the study (Approval number: IR.IAU.SRB.REC.1401.362). The study was conducted according to ethical guidelines and principles.

### Cell culture

The Cell Bank of Pasteur Institute of Iran provided the MDA-MB-231 and MCF-7 cell lines. Dulbecco's Modified Eagle's Medium F12 (DMEM-F12) (Bio-Idea, Iran) with 10% fetal bovine serum (FBS) (Bio-Idea, Iran) under standard cell culture conditions was used as the culture environment at 37 °C in a 5% humidified CO<sub>2</sub> atmosphere.

### Animal

Female BALB/c mice (4–8 weeks) (25–30 g) were procured from Shahid Beheshti University. To ensure the health of the mice, blood sampling was done and blood factors such as RBC (red blood cell), and WBC (white blood cell) were checked. The mice were kept in the Research Center of Tehran University under controlled temperature and humidity conditions with 12 h of ambient light in ventilated and pathogen-free cages. The mice were provided with food and water ad libitum. Three mice were included in each study group for statistical analysis. All mice were labeled, and each treatment group was kept in a separate cage. The head of the laboratory and the authors of the article were aware of all animal studies. Animal experiments were performed following NIH standards approved in 2010 and the protocol of working with laboratory animals approved by the Tehran University of Medical Sciences. This study is in accordance with the ARRIVE guidelines.

### Primary cell isolation

The human CAFs were isolated from tumor samples of 10 individuals diagnosed with invasive ductal carcinoma (IDC) of the breast and normal fibroblast (NFs) were isolated from the non-tumoral area of the same patient. The specimens were thoroughly rinsed twice using PBS and 1% penicillin/streptomycin solution (BIO-IDEA, Iran). The tissues were cut into small pieces (nearly 1–2 mm<sup>2</sup>) and transferred to microtubes containing 1 ml collagenase (5 mg/ml) (Gibco, CA, USA). The mixture of tissue and collagenase was incubated for 90 min at 37 °C in a 5% CO<sub>2</sub> atmosphere. The resultant suspension was passed through a 70 µm mesh (Biofill) and centrifuged with the mixture of DMEM-F12 with 20% FBS. The cells were resuspended in DMEM-F12 with 10% FBS to remove the enzyme and then cultured in T-25 flasks at 37 °C in a 5% CO<sub>2</sub> atmosphere. The medium was replaced after three days to remove floating cells. For CAFs and NFs validation, immunocytochemistry (ICC) staining was applied. To this end, CAFs and NFs were cultured in a 24-well plate in DMEM-F12 medium and incubated at 37°C with a 5% CO<sub>2</sub> atmosphere and 98% humidity conditions for 24 h. On the second day, the wells were rinsed using PBS and dried at room temperature (RT) for 15 min. Then the cells were fixed by adding 400 µl paraformaldehyde and washed twice using PBS. In the next step, wells were blocked by 5% goat serum for 1 h at RT, washed three times using PBS, and incubated with the anti-VIMENTIN antibody (bioscience, San Diego, Western US) at a concentration of 20 µg/ml in 1% Bovine Serum Albumin (BSA) with Tris Buffered Saline (TBS) at RT for 1 h. Afterward, the wells were subjected to 5 min of 100 µl nucleo-staining by DAPI (4',6-diamidino-2-phenylindole) (1 µg/ml) (Calbiochem, USA), rinsed by PBS, and examined under a fluorescent microscope (Olympus, Japan). CAFs were characterized through fluorescence-activated cell sorting (FACS) Caliber (BD Biosciences) using antibodies against CD31, CD45, and CD90 (BioLegend, San Diego, CA).

For MSC isolation, connective tissue and blood were removed from the adipose tissue using a blade and scissors, and 0.2 mg/ml collagenase was added to the tissue. It was then incubated for 40 min at 37 °C in a shaking incubator. Subsequently, 5 ml of medium was added, and the solution was centrifuged at 427 g for 15 min. The resulting pellet was cultured in a 25 cm<sup>2</sup> flask in DMEM-F12 medium supplemented with 1% penicillin/streptomycin and 20% FBS. Spindle-shaped primary MSCs appeared and the medium was replaced after four days. ADMSCs were phenotyped using FACS Caliber (BD Biosciences) using CD45, CD34, CD90, and CD73 antibodies (BioLegend, San Diego, CA).

To evaluate the differentiation ability of MSC to adipocytes, cells ( $1 \times 10^4$  cells/well) were seeded in a 96-well

plate with adipogenic differentiation medium (DMEM containing 0.5 mM 3-isobutyl-1-methyl-xanthine, 10 µg/ml recombinant insulin, 1 µM dexamethasone, and 10% FBS) (Gibco, United States) for two days. Then fresh DMEM-HG containing 10% FBS was replaced with the culture medium for 2–3 days. The cells were fixed in 4% paraformaldehyde for 30 min and Oil Red O stain was used as an index of intracellular lipid aggregation to assess adipocyte formation.

To evaluate the differentiation ability of MSC to osteocytes,  $1 \times 10^4$  cells/well were seeded in a 96-well plate in an osteogenic induction medium (ascorbic 0.3 mM, β-glycerophosphate 10 mM, D-MEM containing dexamethasone  $1 \times 10^{-8}$  M, and 10% FBS) (Gibco, United States). After 14 days of culture, the cells were fixed in 4% paraformaldehyde for 30 min, and then stained with alizarin red to assess calcium aggregation was performed.

To evaluate the differentiation ability of MSC to chondrocytes, cells ( $1 \times 10^4$  cells/well) were seeded in a 96-well plate in a chondrogenic differentiation medium (100 mM sodium pyruvate, 50 µg/ml L-ascorbic acid 2-phosphate, 40 µg/ml proline,  $10^{-7}$  M dexamethasone, 2% fetal bovine serum, ITS + premix in DMEM-HG basic medium, and 1% penicillin–streptomycin (Gibco, United States). The cells were fixed in 4% paraformaldehyde for 30 min after 14 days of culture, and Alcian blue as an index of acidic proteoglycan was used for assessing chondrocyte formation.

### Exosome isolation and identification

To isolate exosomes, ADMSCs and CAFs were cultured in T-75 flasks and incubated at 37 °C in a 5% CO<sub>2</sub> atmosphere. At 80–90% confluency of the cells, fresh DMEM-F12 was added and the medium was left to rest for 48 h.

The Exosome Isolation Kit (AnaCell, Iran) was used for exosome extraction. Briefly, the cultured fluid was centrifuged at 855 g for 10 min. To precipitate dead cells, the supernatant was filtered by using a 0.22 µm filter and reagent A through 5 min of vortex. After formation of a cloudy solution, it was incubated at 4 °C overnight. Then, it vortexed for 1 min, and the mixture was centrifuged at 855g for 40 min at 4 °C to collect the exosomes. In addition, 200 µl of reagent B was added to obtain exosomes. To isolate exosomes from patients and normal serums, blood samples were received in serum separating tubes and immediately centrifuged at 855 g for 10 min. Exosomes were then isolated using an exosome extraction kit (Anacell, Iran) following the mentioned protocol. The suspended exosomes were stored in a microtube at -80 °C for the next experimental steps.

The distribution of exosomes in terms of size was studied using Dynamic Light Scattering (DLS). In total, 50 µL of the exosome was diluted in 1450 µL PBS. The exosome

size and zeta potential were measured at 25 °C using Nano Zetasizer (Malvern Instruments Ltd., UK).

For morphologic evaluation, a scanning electron microscope (SEM) (Seron Technologies AIF2100) was used. On a 1cm<sup>2</sup> microscope slide, 5 µL of exosomes were recorded, dried, and then coated in gold using physical vapor deposition (PVD). The accelerating voltage was 25 kV and the bicinchoninic acid (BCA) Protein Assay kit was employed to measure the amount of protein in the vesicles (Thermo Scientific, Massachusetts, US). To determine vesicle concentration, 50 µL of exosomes were used.

Exosome markers were analyzed by assessing 100 µL of the exosome sample solution in test tubes, one conjugated with a fluorescent dye and 100 µL of exosome sample solution without staining. Exosomes were divided into these tubes and then treated at 4 °C for 30 min with 5 µL of antibodies (CD81 and CD63 antibody which are specific markers for extracellular vesicles) (BioLegend, San Diego, CA). Subsequently, a FACSCalibur flow cytometer was employed to examine the size distribution of 100 nm-sized beads (BD Biosciences), and then data analysis was done in FlowJo software.

Moreover, an enzyme-linked immunosorbent assay (ELISA) was utilized to identify and detect CD9 and CD63 proteins in the mixture. To achieve this, each well was exposed to 100 µL of coating solution and incubated at 37 °C for one hour. Next, 250 µL of blocking buffer was introduced and the sample were rinsed for three times with 300 µL of wash buffer before being incubated for 1 h at 37 °C. Then, 100 µL of the prepared standard and sample dilution were added to the wells and incubated for 40 min in a coating buffer. Afterward, 3, 3.5, and 5 Tetramethylbenzidine (TMB) substrate was introduced, and the absorbance was measured after 30 min at 450 nm (Jenway 6305 spectrophotometer, Vietnam).

Western blot was used to detect protein marker CALNEXIN (ab22595, Abcam, UK) on exosome or whole cell lysate. Briefly, to separate the proteins with different molecular weights in the Bio-Rad Electrophoresis System (California, USA) exosomes and whole cell lysate were loaded into 10% SDS-polyacrylamide gel, and a voltage of 90 volts was applied. PVDF membranes (Sigma-Aldrich, Germany) were blocked with a blocking buffer for 2 h in a shaker, washed by TBST, and incubated with antibody against CALNEXIN at 4 °C for 24 h. The blots were then incubated using horseradish peroxidase-conjugated anti-rabbit secondary antibody (Abcam) for 2 h for signal visualization. The bound of protein was detected by employing the ECL prime Western blotting detection (GE Healthcare).

#### **Dox loading into MSC-Exos**

A 500 µL solution of MSC-Exos (0.45 mg/mL) was appropriately mixed with Dox (Ebedoxo, 50 mg/25 mL) in a 1 mL volume, followed by dilution using PBS (pH 7.4) to achieve final concentrations of 1, 1.25, 2.5, and 4 µM. The sonication procedure was performed using an ultrasonic probe (BANDELIN SONOPULS GM3200, Berlin) immersed in the mixture. Six cycles of the full procedure were carried out, with a frequency of 20 kHz, amplitude of 20%, and 30 s on and off with a 2-min break between each cycle. The procedure was performed in an ice bath to prevent heating of the sample. To recover the exosomal membrane, the fluid was incubated for 30 min at 37 °C. Non-entrapped Dox was separated by centrifugation at 14,000 g for 30 min.

The concentration of Dox within the extracted exosomes was assessed by utilizing Radioimmunoprecipitation assay buffer (RIPA buffer) for dissolving Exo-Dox. Optical density (OD) measurements were conducted at 490 nm subsequent to the dissolution of Exo-Dox. Finally, the morphological characteristics of Exo-Dox were studied utilizing transmission electron microscopy (TEM), (Philips EM-208 S, 100 kb Netherlands). A sample solution of 400 µL was dropped on Formvar-carbon copper grids, followed by negative staining with uranyl acetate (1%) for 2 min prior to air drying.

#### **Cytotoxicity study**

The cytotoxicity effect of free Dox, free MSC-Exos, and Exo-Dox on NFs, MDA-MB-231, MCF7, CAFs, and co-culture of MDA-MB-231 and MCF-7 cells with CAFs were evaluated through MTT assay. Briefly, the cells were seeded (5,000 cells/well) in 200 µL of 10% medium in a 96-well plate and incubated for 24 h. Afterward, the cells were exposed to different concentrations of Dox (2.5, 5, 10, 20 and 40 µM) for 24 and 48 h, Exo-Dox (0.625, 1.25, 2.5, 5, 10, 20 and 40 µM) and free MSC-Exos for 48 and 72 h at 37 °C with 5% CO<sub>2</sub>; 3 replicates were done for all groups. Three wells per group were designated as control groups (untreated cells). After each incubation period, the media were removed, and the cells were incubated with 100 µL of MTT reagent (Thiazolyl Blue Tetrazolium Bromide powder, Sigma, Germany). The formazan crystals formed were dissolved after 4 h by adding 100 µL of dimethyl sulfoxide (DMSO, Sigma, Germany). The absorbance level was determined at 570 nm using an ELISA plate reader (Biotek, Vermont, USA). The rate of cell growth inhibition (IR) was determined as follows:

Inhibitory rate (%) =  $(1 - \text{mean OD value in the experimental group} / \text{mean OD value in the control group}) \times 100\%$ .

The IC<sub>50</sub> values of Dox and Exo-Dox were estimated based on the OD value for each group of cells.

### Cell uptake assay

The cellular uptake of Exo-Dox by MCF-7 cells was assessed utilizing a fluorescence microscopy-based method. Specifically, MCF-7 cells were seeded at  $1 \times 10^4$  cells/well density in a 24-well plate and incubated overnight (37 °C, 5% CO<sub>2</sub>). After removing the media, 100 µl of Exo-Dox (2.5 µM) and 100 µl of 10% DMEM-F12 medium were added to the wells and further incubated for 4 hrs. Then, the cells were rinsed with 50 µl PBS and fixed with 50 µl paraformaldehyde (4%) for 15 min. The nuclei of the cells were examined with 20 µl of DAPI (Sigma-Aldrich) at 1 µg/ml concentration. Cellular uptake of Exo-Dox was visualized using an inverted fluorescence microscope (BLACKL. 5000 MET, MONSA, Italy).

### Real-time PCR

The expression levels of lncRNA *H19* and *UCA1* were evaluated by q-RT PCR in various groups including isolated CAFs and NFs, CAF exosomes, and serum exosomes of patients. Additionally, the expression of lncRNA and *TP53* in the cells (MCF-7, MDA-MB-231, and co-culture of MCF-7 and MDA-MB-231 with CAFs) treated with Exo-Dox and Dox was investigated. To determine the value specificity of these lncRNAs, the receiver operating characteristic (ROC) graph was assessed.

Total RNA was extracted using Kiazol RNA (KiaZist, Iran). The concentration and OD ratio of isolated RNAs were defined spectrometrically (BioTek, USA). SMOBIO Technology kit was utilized to synthesize cDNA. According to the protocol, 2 µl RNA, 1 µl dNTP mix, 1 µl random hexamers (100 µM), and 6 µl diethylpyrocarbonate (DEPC)-Treated H<sub>2</sub>O were mixed well and incubated at 70 °C for 5 min. Afterward, 4 µl 5X RT Buffer, 4 µl DEPC-Treated H<sub>2</sub>O, 1 µl RNAok RNase Inhibitor, and 1 µl Reverse Transcriptase were combined and added into the mixture. The solution was then incubated (25 °C, 10 min) at 50 °C for 50 min. In the termination step, the incubation was at 85 °C for 5 min.

Real-time PCR was carried out using 2x SYBER green Master Mix (Sinacolon, Iran), and a RotorGene Q machine (Corbett, Germany) was used to run the PCR cycles. The amplification protocol started with a denaturation step (95 °C, 10 min) with 40 denaturation cycles at 95 °C for 20s, annealing at 55 °C for 30s, and an extension at 72 °C for 20s. The melting temperature was

72–95 °C. The primers were developed by the Gene Runner (v.6.5.52) software (Table 1). All experiments were performed in duplicate, and *β-ACTIN* was utilized as an internal control. The  $2^{-\Delta\Delta C_t}$  technique was employed in the real-time PCR data analysis.

### Live and dead assay

For acridine orange (AO) staining, MCF-7, MDA-MB-231, CAFs, co-cultures of MCF-7/CAF and MDA-MB-231/CAF were seeded at  $5 \times 10^3$  cells/well density in 200 µl of culture medium in 96-well plates. After 24 h of incubation, each cell group received treatment with the respective IC<sub>50</sub> concentration of Dox and Exo-Dox. All experiments were conducted in triplicate. Following the incubation period, the cells were washed with PBS and fixed with 4% paraformaldehyde. Nuclei were then stained with 50 µl of AO fluorescent stain (Sigma-Aldrich) in the dark for 3 minutes. A fluorescence microscope (BLACKL. 5000 MET, MONSA, Italy) was used to visualize live and dead cells. ImageJ software (version. 1.8.0) was used to analyze the images and determine the percentage of live and dead cells in each group.

### Apoptosis assay

MCF-7, MDA-MB-231, and co-culture of MDA-MB-231/CAF and MCF-7/CAF cells were seeded at the density of  $25 \times 10^4$  cells per well in 3 ml of the medium in 6-well plates for 24 h. The cells were then exposed to their respective IC<sub>50</sub> concentrations of Dox and Exo-Dox. An Annexin V-FITC apoptosis detection kit (BioLegend, San Diego, CA) was used to analyze cell apoptosis according to the producer's instructions. After detachment from the culture plate, the cells were collected via centrifugation, and a binding buffer (1X) was added to the cell sediment. Each tube was supplemented with 3 µl of Annexin V-FITC before the entire batch was incubated at 4°C in the dark. Afterward, the cells were centrifuged, and the cell pellets were suspended in 500 µl of the binding buffer. Finally, the cells were analyzed using flow cytometry using a binding buffer at 520 nm and 617 nm for Annexin V-FITC and Propidium Iodide (PI), respectively.

### Migration assay

To examine the effects of treatment on cell migration, a scratch-wound cell migration assay was performed on

**Table 1** Primers used in this study for real-time PCR

lncRNA	Forward	Reverse	Product-Size (bp)	Accession number
<i>β-ACTIN</i>	CTCTCCAGCCTTCCTTCT	AGCACTCTGTTGGCGTACAG	116	NM_001101.5
<i>UCA1</i>	TTTGCCAGCCTCAGCTTAAT	TTGTCCCATTTTCCATCAT	186	NR_015379.3
<i>H19</i>	GCCTTCCTGAACACCTTA	GAGCCGATTCTGAGTC	123	NR_002196.2
<i>P53</i>	AGTATTTGGATGACAGAAA	TTACCACTGGAGTCTTC	181	NM_001126114.3

MDA-MB-231/CAFs co-cultured, respecting an invasive group of breast cancer cells.

Briefly, a 6-well plate was used to seed the cells ( $3 \times 10^5$  cells per well), which were left to grow overnight. Afterward, each well was scratched using a sterile pipette tip. The cells were then washed twice with PBS. One well was left untreated while another well was treated with the IC50 concentration and incubated ( $37^\circ\text{C}$  in a 5%  $\text{CO}_2$ ). The migration of cells into the scratch wound was assessed by imaging the cells using an inverted microscope at 0 and 24 h (Nikon, ECLIPSE, TS100).

#### In vivo distribution of intravenously injected Exo-Dox

Four to eight-week-old female BALB/c nude mice received  $10^6$  MDA-MB-231 and CAF cells mixed with Matrigel (BD, Bioscience, CA, USA) at a ratio of 1:1 in the right mammary gland through subcutaneous injection to determine the biodistribution of Exo-Dox. 25 nmol of ODAP-490 in a volume of 100  $\mu\text{L}$  PBS and ODAP-490 labeled exosomes were IV injected into tumor-bearing mice when the volume of tumors reached 0.1  $\text{cm}^3$  in about six days. By using the Bio-Real Quickview 3000 in vivo Imaging System (Bio-Real Sciences), fluorescent images were obtained at 1, 2, and 4 h after injection.

#### In vivo antitumor assays

To investigate the anti-tumor effects, the BALB/c nude mice were anesthetized by intraperitoneal injection of

10 ml ketamine and 15 ml xylazine and inoculated with MDA-MB-231 and CAF cells ( $1 \times 10^6$  cells in 100  $\mu\text{L}$  PBS). Five days after the injection of cells, tumor-bearing mice ( $1\text{mm}^3$ ) were sorted randomly into four treatment groups ( $n = 3/\text{group}$ ) including PBS, MSCs-Exo, Exo-Dox, and Dox (a Dox equivalent of 5 mg/kg). The mice were injected intravenously through the tail vein with an interval of two days for five times total. The tumor volume (TV) was calculated as follows:

$$\text{TV (mm}^3\text{)} = (\text{height} \times \text{length} \times \text{width}) \times 0.5 \text{ mm}^3.$$

Finally, the mice were sacrificed, and the major organs (liver, heart, kidney) were weighed. The tumor tissues and organs were fixed in 4% paraformaldehyde (PFA) and stained with hematoxylin and eosin (H&E). Immunohistochemical (IHC) staining was performed on tumor tissues extracted from treated mice using an automated immunostainer (Leica Bond-III, Leica, Buffalo Grove, IL). Primary antibodies against Ki-67 and CD45 (Abcam, Cambridge, MA) were used for staining (tin plated). The stained tissue sections were then analyzed using the Aperio ScanScope Image Analysis System (Aperio, Vista, CA).

#### Statistical analysis

Graph Pad Prism (v.8) was used to perform the student's t-test ( $p\text{-value} < 0.05$ ) and the experiments were carried out three times.

## Results

### Demographic analysis

The clinicopathological specifications of the subjects are presented in Table 2. The mean age of the breast cancer participants was 59.5 years. All cases had invasive ductal carcinoma (IDC) with positive progesterone (PR), negative estrogen (ER), and human epidermal growth factor receptor 2 (HER-2). Half of the participants had a tumor size less than or equal to 2 cm. More than 25% of patients had lymph node involvement. All patients were in the early stages of breast cancer and no distant metastases (M0) were observed in any of the cases.

### Characterization of primary cells

The isolated MSCs demonstrated a spindle-shaped morphology. The multipotent capability of MSCs was determined by culturing in appropriate culture mediums for adipocyte, osteocyte, and chondrocyte induction (Fig. 1A and S. 2 A)). Phenotypic marker analysis revealed that MSCs were negative for CD45 and CD34 (Fig. 1B and S. 2B)), and positive for CD90 and CD73 (Fig. 1C). CAFs showed a spindle-shaped fibroblast morphology (Fig. 1D). The ICC results of cultured CAFs and NFs cells showed that CAFs were more positive for VIMENTIN (Fig. 1E). The phenotypic marker analysis indicated that

**Table 2** Demographic data of patients

Clinicopathological characteristics	Number	Percentage
Age		
< 50	4	40%
> 50	6	60%
Type		
Invasive ductal carcinoma	10	100%
Invasive lobular carcinoma	0	0%
TNM stage		
1	5	50%
2	5	50%
3	0	0%
Differentiation grade		
G1	4	40%
G2	6	60%
G3	0	0%
Lymph node involvement		
Positive	3	30%
Negative	7	70%
HER-2 status		
Positive	0	0%
Negative	10	100%
Tumor size		
< 2 cm	5	50%
> 2 cm	5	50%

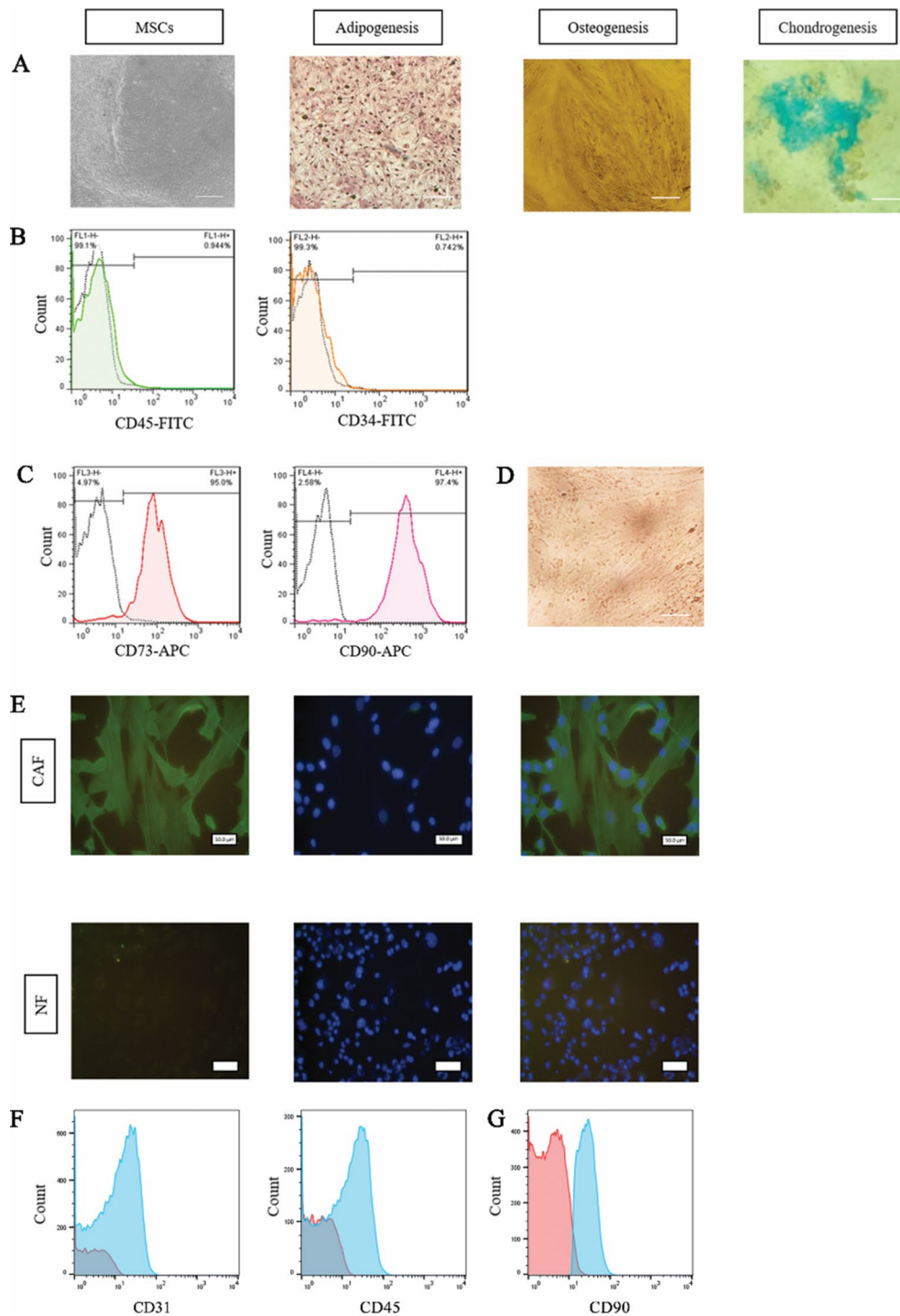


**Fig. 1** Characterization of ADMSCs and CAFs. **(A)** Cropped microscopy image of AMSCs phenotype, scale bar = 50  $\mu$ m, magnification, 10X, adipogenesis: oil red O staining, osteogenesis: alizarin red staining, chondrogenesis: Alcian blue staining. **(B)** Immunophenotypic analysis of cultured AMSCs with monoclonal antibodies. Findings indicated that the cells were negative for CD45 and CD34 markers, and **(C)** positive for MSC markers CD73, and CD90. **(D)** Cropped microscopy image of CAFs phenotype, scale bar = 50  $\mu$ m, magnification, 10X. **(E)** Immunophenotypic analysis of cultured CAFs with monoclonal antibodies. (1) blue, DAPI, (2) green, VIMENTIN. CAFs had higher levels of VIMENTIN positivity than NFs, scale bar = 50  $\mu$ m. **(F)** Flow cytometry analysis of cultured CAFs. Cells negative for CD31 were found non-endothelial, while CD45-negative cells were confirmed as non-leukocytes. **(G)** CD90 serves as a key marker for fibroblasts, confirming its fibroblastic identity. The figures are based on three independent experiments

CAFs were negative for CD31 and CD45 (Fig. 1F) and positive for CD90 (Fig. 1G).

### Characterization of exosomes

Exosomes derived from MSCs and CAFs were also characterized. Scanning electron microscopy (SEM) analysis revealed that the exosomes which had an average size of between 40 and 200 nm were disc-shaped (Fig. 2A and S. 3 A). The average size of the exosomes derived from MSCs and CAFs were obtained equal to 180 nm and 149 nm based on zeta sizer data, and the reported zeta potential was  $-12.4$  mV and  $-7.5$  mV, respectively (Fig. 2B and S. 3B). The expression of some key exosomal markers, including CD9 and CD63, was confirmed by ELISA (Fig. 2C). Phenotypic marker analysis revealed that MSCs-derived exosomes were negative for CD81 and positive for CD63 (S. 3 C). These results showed that both kinds of exosomes were isolated successfully. The protein amount of CAFs and MSC exosomes were quantified using the BCA assay equal to 1.5 and 0.45 mg per ml respectively. Moreover, no CALNEXIN (endoplasmic

reticulum marker) expression was observed in exosomes based on Western blot (Fig. 2D and S. 4).

### Dox loading and Exo-Dox characterization

The amount of encapsulated Dox was determined using intrinsic fluorescence analysis at 490 nm by using diagrams of different concentrations of Dox (S. 5). The finding indicated that  $\sim 59\%$  of Dox was loaded into the exosomes (Fig. 3A). The TEM results demonstrated the preservation of the exosome membrane integrity (Fig. 3Bii). Furthermore, the color change of exosomes to dark gray provided additional confirmation of the successful encapsulation of Dox within the exosomes (Fig. 3Biii). To investigate the cellular uptake,  $2.5 \mu\text{M}$  of Exo-Dox was incubated with MCF-7 cells for 4 h. Fluorescent microscope images showed that Exo-Dox entered into cells perfectly (Fig. 3C).

### Cytotoxicity and antitumor effects of Exo-Dox

Figure 4A and B display the cell viability of NFs, MDA-MB-231, MCF-7, CAFs, co-culture of MDA-MB-231

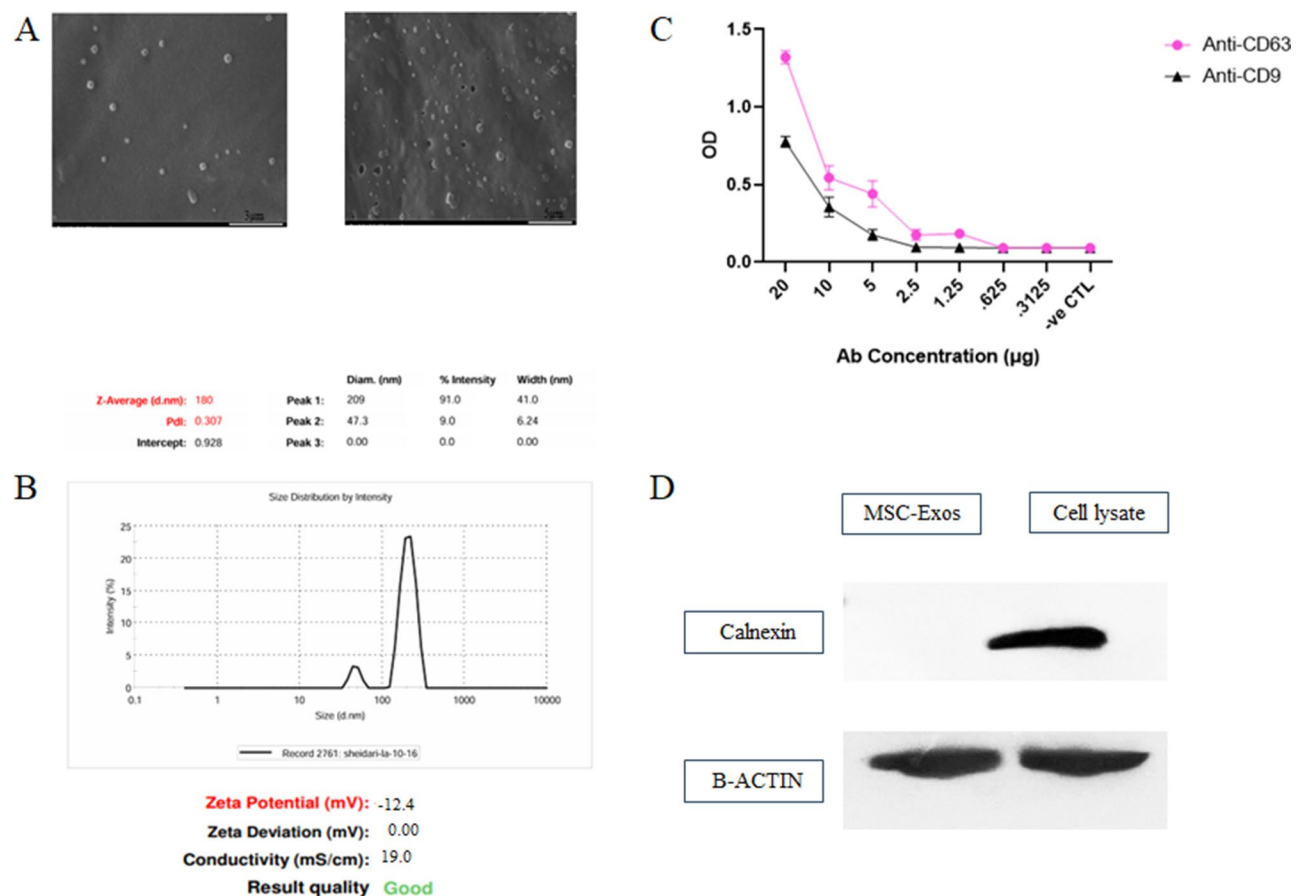


**Fig. 2** Characterization of MSCs-derived exosomes. **(A)** SEM micrograph of MSCs-derived exosomes, low magnification, scale bar =  $5 \mu\text{m}$  and high magnification, scale bar =  $3 \mu\text{m}$ . **(B)** Size distribution by number of MSCs-Exo. **(C)** Elisa analysis of positive exosomal CD markers in both isolated exosomes: (1) pink graph, CD63 expression in exosomes lysate, (2) black graph, CD9 expression in exosomes. **(D)** Western blot analysis for CALNEXIN (endoplasmic reticulum marker) expression in cellular and exosomal lysate (Cropped). experiments were done at least three independent times

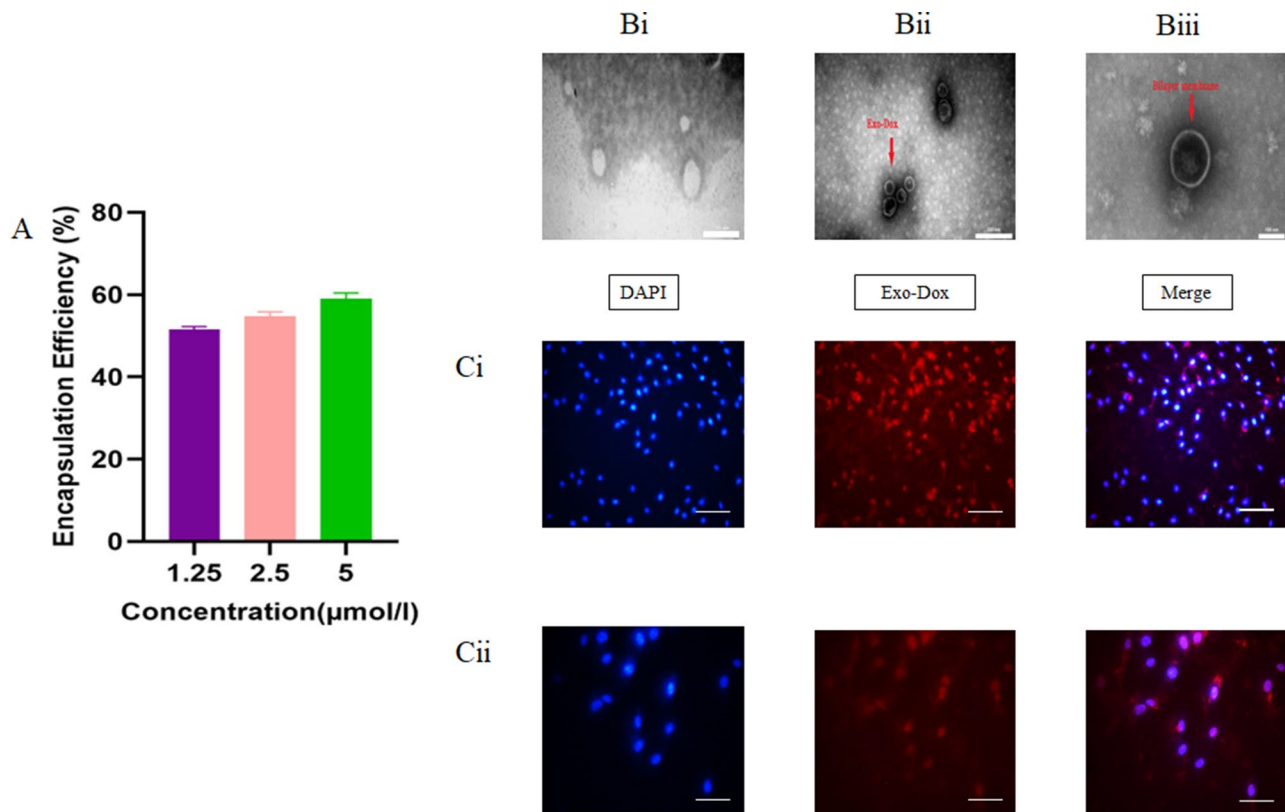


**Fig. 3** Dox loading confirmation. **(A)** Dox standard curve. Emission and excitation were determined using a fluorimeter at 595 and 480 nm, respectively. **(B)** Characterization of Exo-Dox using TEM images. **(Bi)** TEM image of Msc-derived exosomes. **(Bii)** The lipid membrane and integrity of exosomes after Dox loading are clearly visible, scale bar = 200 nm. **(Biii)** color change to dark gray could be observed for Exo-Dox, scale bar = 100 nm. **(C)** Fluorescent microscopy images of the drug-loaded Exo intracellular distribution. Blue fluorescence indicates the cell nucleus and red fluorescence indicates Exo-Dox scale bar = 50 μm **(Ci)** magnification, 20X. **(Cii)** magnification, 40X. The figures are based on three independent experiments

with CAFs, and co-culture of MCF-7 with CAFs treated with free Dox for 24 and 48 h. Free Dox reduced the cell viability of all cell types compared to the control group. The inhibitory effects of Dox was particularly prominent in MDA-MB-231, MCF-7 cells and co-culture of MDA-MB-231 and MCF-7 with CAFs, with cell viability of approximately 26.9%, 30.3%, 71%, and 30.35% respectively in 48 h.

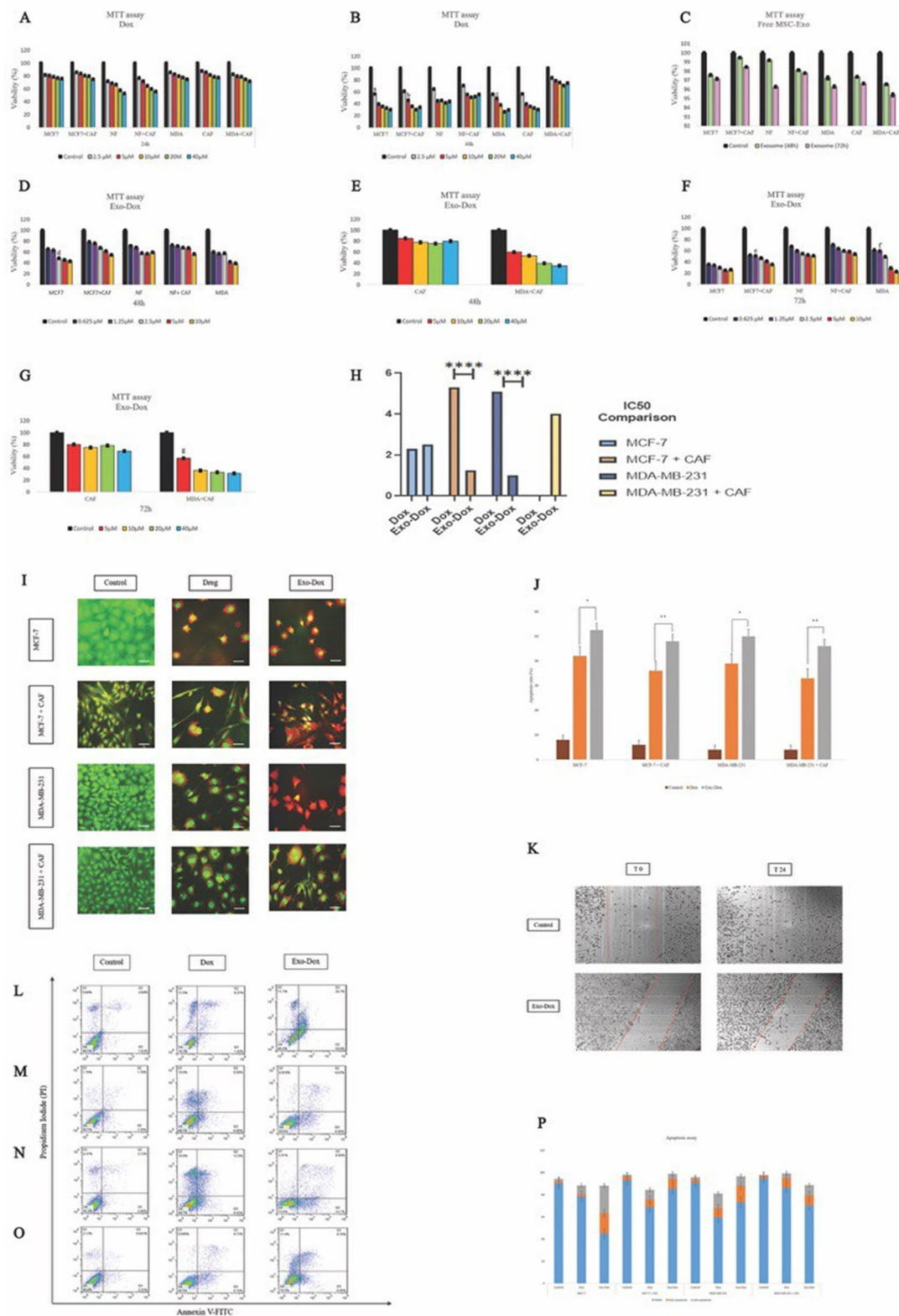
The results showed that free MSC-Exos did not affect cell viability in all cell types. (Fig. 4C) In contrast, Exo-Dox exhibited a significant cytotoxic effect on BC cells, which was concentration depended. The MTT assay revealed that the cytotoxic effect of Exo-Dox was sustained for 72 h in all cell types, indicating that the release of Dox from the exosomes was prolonged (Fig. 4D, E, E, and G). Additionally, the half-maximal inhibitory dose (IC<sub>50</sub>) of Exo-Dox was significantly less than free Dox in all groups ( $P < 0.0001$ ), except for MCF-7 cells (Fig. 4H).

Table 3 summarizes the IC<sub>50</sub> values of free Dox and Exo-Dox for NFs, MDA-MB-231, MCF-7, CAFs, co-culture of MDA-MB-231 with CAFs, and co-culture of MCF-7 with CAF cells. The results revealed that Exo-Dox had a lower IC<sub>50</sub> value than free Dox in all cell

types, except for MCF-7 cells. A comparison between the subgroups of the MTT assay is shown in S. 6.

Breast cancer cells were exposed to the IC<sub>50</sub> value of Exo-Dox and Dox to evaluate their anticancer effects. Exo-Dox had a significant impact on both triple positive and triple negative BC (TNBC) cells (Fig. 4I and S. 7). The graph demonstrates that all Exo-Dox treated groups had apoptosis rates that were significantly higher than free Dox ( $P < 0.01$ ) (Fig. 4J). The apoptotic percentages for MDA-MB-231 cells were 39% and 50% for Dox and Exo-Dox treatments respectively. Treatment of MCF-7 cells with Dox resulted in an apoptotic percentage of 42%, whereas treatment with Exo-Dox led to a significantly higher apoptotic percentage of 52.5%. Co-culture treatment of MDA-MB-231 and CAFs with Exo-Dox resulted in an apoptotic percentage of 46%. Treatment of the MCF-7 and CAFs co-culture with Dox and Exo-Dox resulted in apoptotic percentages of 36% and 48% respectively.

A wound was created by sliding a yellow plastic pipette tip across the surface of nearly 70% confluent MDA-MB-231 with CAF co-culture. At 0 h, the wound diameters of the Exo-Dox treated and control cells were



**Fig. 4** (See legend on next page.)

(See figure on previous page.)

**Fig. 4** Cytotoxicity and antitumor effects of Exo-Dox. **(A)** MDA-MB-231, MCF7, CAFs, co-culture of MDA-MB-231 with CAFs, co-culture of MCF-7 with CAFs and co-culture of NFs with CAFs for 24 h. **(B)** 48 h. (a, b, and c) values close to IC50 of MCF7, co-culture of MCF-7 with CAFs, and MDA-MB-231. **(C)** Free MSC-Exo for 48 and 72 h. **(D and F)** treated cells by Exo-Dox for 48 and 72 h. (d, e and f) values close to IC50 of MCF7, co-culture of MCF-7 with CAFs, and MDA-MB-231. **(E and G)** MDA-MB-231 and co-culture of MDA-MB-231 with CAFs treated by Exo-Dox for 48 and 72 h. (g) value close to IC50 of co-culture of MDA-MB-231 with CAFs. **(H)** IC50 comparison between Dox and Exo-Dox. IC50 of co-cultured MCF-7 with CAFs and MDA-MB-231 cells treated by Exo-Dox was 4.24 and 5.1-fold lower than treated by Dox ( $P < 0.0001$ ). **(I)** Live and dead assay (Cropped images). MDA-MB-231, MCF7, CAFs, co-culture of MDA-MB-231 and MCF-7 with CAFs cells, green fluorescence and red fluorescence show live and dead cells respectively, scale bar = 10  $\mu\text{m}$ , magnification, 40X. **(J)** Graph of apoptosis rate comparison between MDAMB-231, MCF7, CAFs, and co-culture of MDA-MB-231 and MCF-7 with CAFs following treatment with Dox and Exo-Dox. The apoptotic rate of cells is calculated based on the results of AO staining. Apoptosis Rate (%) = (number of apoptotic cells/total number of cells)  $\times$  100. The apoptosis rate was increased significantly in cells treated by Exo-Dox compared with Dox ( $P < 0.05$ ). **(K)** micrographs of living cultures of MDA-MB-231 with CAF cells in a migration assay. The control sample and Exo-Dox treated sample at 0 and 24 h. Treatment with Exo-Dox on co-culture of MDA-MB-231 with CAFs inhibits cell migration. **(L)** MCF-7 cells are exposed to their own IC50 dosage of Dox and Exo-Dox. From left to right each column refers to control, Dox, and Exo-Dox. **(M)** Co-culture of MCF-7 with CAFs. **(N)** MDAMB-231. **(O)** Co-culture of MDA-MB-231 with CAFs. **(P)** Diagrams show that in all groups, apoptosis increased in Exo-Dox treated cells compared to Dox treated cells. The results are based on three independent experiments. T-test  $*P \leq 0.05$ ,  $**P \leq 0.01$ ,  $***P \leq 0.0001$

measured. The co-culture of MDA-MB-231 and CAFs in the control group migrated to cover the area created by the wound. In contrast, after 24 h of growth in the incubator, the Exo-Dox treated cells were unable to migrate, and the wound remained open (Fig. 4K). These results indicate that Exo-Dox suppressed the cells' ability to migrate.

The proportion of apoptotic MCF-7 cells treated with Dox was 10.14%, whereas the percentage of apoptotic cells treated with Exo-Dox was significantly higher at 43.3%. MCF-7 cells were the most sensitive to both Dox and Exo-Dox treatments compared to other groups. For Dox and Exo-Dox treatments, the apoptotic percentages for MDA-MB-231 cells were 21.33% and 23.3%, respectively. Exo-Dox treatment caused an 18.14% increase in apoptosis in the MDA-MB-231 and CAFs co-culture. Dox and Exo-Dox treatments caused apoptotic effects of 15.43% and 13.52% respectively, in the MCF-7 and CAFs co-culture (Fig. 4L-P).

#### Real-time PCR

Compared to normal serum exosomes, real-time PCR findings indicated significantly higher expression levels of both *H19* and *UCA1* in serum exosomes of patients ( $P < 0.0001$ ) (Fig. 5Ai, Aii). Moreover, higher expression levels of these lncRNAs were observed in MCF-7, MDA-MB-231, and co-culture of MCF-7 and MDA-MB231 with CAFs and CAFs cells, compared to NFs ( $P < 0.0001$ ) (Fig. 5Bi, Bii). Additionally, both *H19* and *UCA1* expression levels were downregulated significantly in MCF-7, MDA-MB-231, and co-culture of MCF-7 and MDA-MB-231 with CAF cells treated with Exo-Dox ( $P < 0.05$ ) (Fig. 5Biii). Still, the expression of the *TP53* gene considerably increased in the mentioned treated cell groups ( $P < 0.0001$ ) (Fig. 5Biv). A comparison between gene expression in subgroups of cells is shown in S. 8.

To further explore the clinical significance of these findings, a heat map diagram was constructed to show the expression levels of both lncRNAs in healthy individuals and breast cancer patients. The findings indicated

that both *H19* and *UCA1* expressions were higher significantly in patients compared to healthy individuals (Fig. 5C). Pearson and Spearman's methods demonstrated that the expression levels of these two lncRNAs had no relationship to each other (Fig. 5D).

Furthermore, our results showed that the up-regulation of these lncRNAs was not related to age, stage, differentiation grade, lymph node metastases, or any other factor. Receiver operating characteristics (ROC) curves of both *H19* and *UCA1* demonstrated their potent breast cancer identification capacities, with area under the curve (AUC) of 1 ( $P = 0.0002$ ), and specificity of 100% (Fig. 5E). Therefore, these lncRNAs can be suitable biomarkers.

#### In vivo visualization of Exo-Dox

The tumor-distribution ability of Exo-Dox was assessed in a tumor xenograft mouse model. Figure 6A and S. 9 demonstrate images at 1, 2, and 4 h post MSC-Exos injection. ODAP-490 labeled exosomes reached and gathered at the breast at 4 h, and since tumorigenesis occurred in the kidney, liver, and spleen, they reached these areas as well.

#### In vivo anti-tumor effect

The anti-tumor effect of Exo-Dox was evaluated using a murine model of BC (Fig. 6B, C). The tumor volumes of the mice were measured at regular intervals. Overall, the tumor volumes of mice receiving Exo-Dox decreased more than those receiving Dox ( $p < 0.05$ ). On the 20th day of treatment, the average tumor sizes were 1.7, 1.5, 0.85, and 0.17 for PBS, MSC-Exo, Dox, and Exo-Dox, respectively. The findings indicated that the tumor size in the Exo-Dox treated group was significantly decreased compared to PBS ( $p < 0.01$ ).

H&E staining of breast tumor tissue demonstrated tumor progression in the control group (PBS). Inflammation and cancer cell division were significantly reduced in the treated mice, especially the Exo-Dox group. Additionally, central necrotic cells around leukocytes were observed in the liver and kidney tissues, but

**Table 3** IC50 of free Dox and Exo-Dox

BC cells	Dox 48 h	Exo-Dox 48 h	Exo-Dox 72 h
MDA-MB-231	5.1		1
MDA-MB-231 + CAFs			4
MCF-7	2.3	2.5	
MCF-7 + CAFs	5.3		1.25

were considerably lower in the Exo-Dox treated group (Fig. 6D). Immunohistochemical staining for Ki-67 and CD45 was utilized to evaluate the proliferative and inflammation index of a tumor, respectively. As depicted in Fig. 6E, our analysis revealed a significantly higher abundance of Ki-67 and CD45 positive cells in the control group compared to the treated groups. These findings indicate that Dox, and Exo-Dox treatments effectively reduced the tumor proliferation rate, and level of inflammation, with the most pronounced effect observed in the Exo-Dox group ( $P < 0.01$ ) (S 10).

## Discussion

BC is a complex and heterogeneous disease that presents different molecular subtypes, including TNBC [18]. The lack of (ER), (PR) and (HER2) receptors in TNBC renders conventional therapies ineffective, highlighting the need for better treatment strategies [19].

Tumor progression and proliferation are regulated by the interplay between tumor cells and their microenvironment. Among the cell types interacting with cancer cells, cancer-associated fibroblasts (CAFs) enhance epithelial cell activity [20]. By producing various substances and establishing direct contact with cancer cells, CAFs can promote drug resistance and metastasis [21]. Several studies have shown that the interaction between CAFs and BC cells is a factor in cancer invasiveness [22]. Additionally, lncRNAs such as *H19* and *UCA1* are linked to drug resistance in several malignancies [23, 24].

Exosomes, natural nanovesicles enclosed by membranes, are released by tumor cells to communicate with neighboring or distant cells in the tumor microenvironment [25]. While the precise mechanisms underlying exosome function remain unclear, studies have reported their significant contributions in the development, invasion, migration, and drug resistance of BC [26]. Exosomes contain a variety of RNAs, including lncRNAs, which can alter gene expression in recipient cells and contribute to the pathogenesis of BC [27].

The exosomes derived from CAFs contain full genomic mitochondrial DNA (mtDNA) and act as onco-signals, promoting hormone therapy resistance in BC [28]. These results also demonstrated that CAF exosomes can

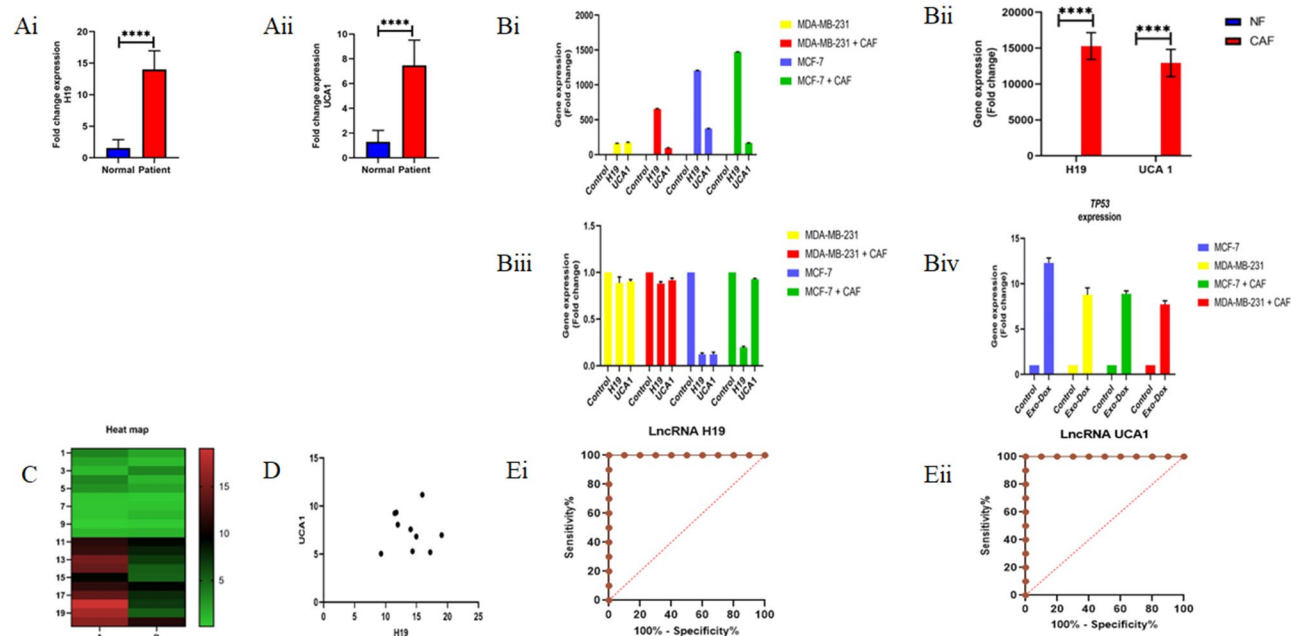


**Fig. 5** The expression level of lncRNA *H19*, *UCA1* and *TP53*. (Ai) *H19* and (Aii) *UCA1* expressions were significantly higher in the serum exosomes of patients compared with serum exosomes of normal ones. (Bi) MCF-7, MDA-MB-231, and co-culture of MCF-7 and MDA-MB-231 with CAFs compared with NFs showed significantly higher expression levels of these lncRNAs ( $P < 0.0001$ ). (Bii) CAFs compared with NFs showed significantly higher expression levels of these lncRNAs ( $P < 0.0001$ ). (Biii) MCF-7, MDA-MB-231, and co-culture of MCF-7 and MDA-MB-231 with CAFs treated by Exo-Dox, the *H19*, and *UCA1* were significantly lower than untreated cells ( $P < 0.0001$ ). (Biv) Upregulation of *TP53* in all treated cells compared to control ones. (C) Heatmap diagram: (A) *H19* and (B) *UCA1* in (0–10) normal and (11–20) breast cancer patients. (D) The correlation between expression level of *H19* and lncRNA *UCA1*. The expression level of *H19* was not correlated to the expression level of *UCA1*. (E) ROC curve. The AUC was 1 ( $P$  value = 0.0002, 95% CI = 1). (Ei) *H19*. (Eii) *UCA1*. All experiments were done at least two times. T-test  $**P \leq 0.01$ ,  $***P \leq 0.001$ ,  $****P \leq 0.0001$

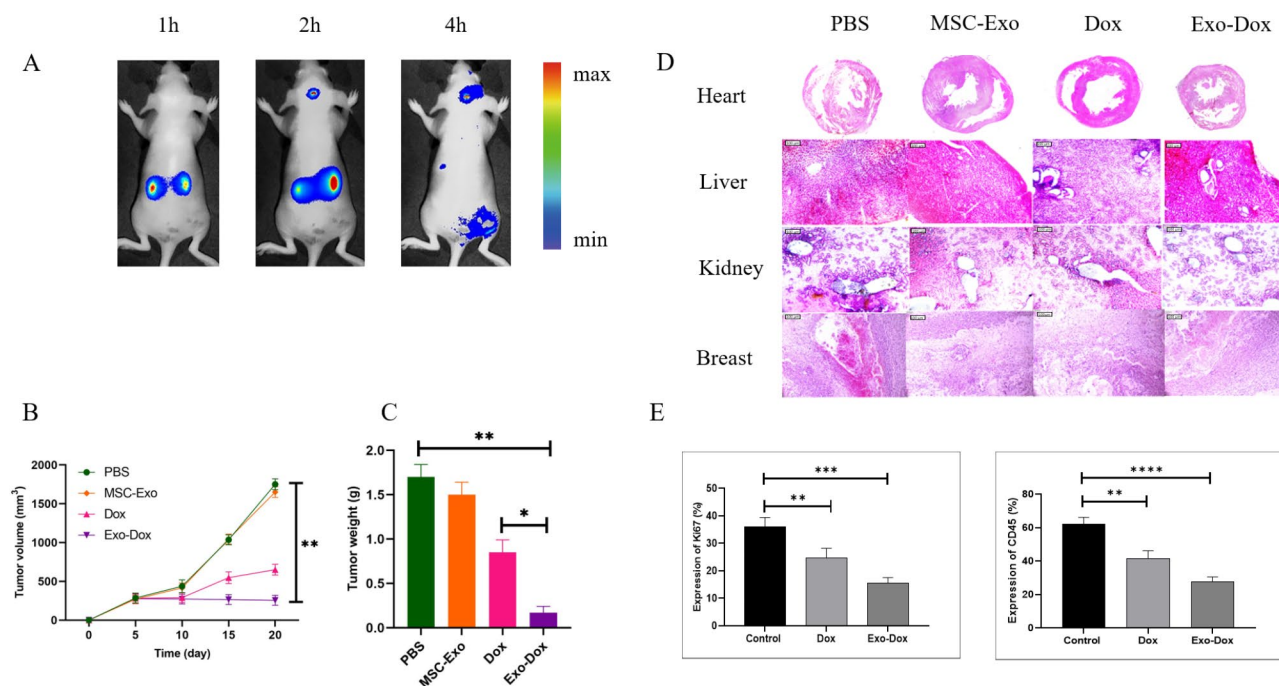


**Fig. 6** The in vivo distribution and anti-tumor effect of Exo-Dox. **(A)** In vivo biodistribution of Exo-Dox in MDA-MB-231 and CAFs tumor-bearing mice. **(B)** Average absolute tumor growth curves of mice injected with different formulations ( $n = 3$ ). **(C)** Weight of excised tumors in mice after 20th day of treatments ( $n = 3$ ). **(D)** H&E-stained MDA-MB-231 tumor-bearing mice following treatments. **(E)** The expression level of Ki-67 and CD45 in breast tumor tissue. The results are based on three independent experiments. Data are shown as mean  $\pm$  SD. \*\* $P < 0.01$ , \*\*\* $P < 0.001$ , \*\*\*\* $P < 0.0001$

significantly increase the expression of various lncRNAs, including *H19* and *UCA1*, which may contribute to drug resistance.

In one of the studies conducted on *UCA1*, the higher expression of this lncRNA was significant ( $p < 0.01$ ) on tamoxifen-resistant cells (LCC2) in comparison with tamoxifen-sensitive cells (MCF-7). In addition, an increased expression in the exosomes obtained from LCC2 cells in comparison with MCF-7 cells was also observed, which was more significant. High expression of *UCA1* plays a role in tamoxifen resistance through suppressing CASPASE-3 and cell apoptosis [29].

A study indicated that *H19* expression was increased significantly in serum samples of BC patients and Dox-resistant BC cells and these cells can transfer resistance to sensitive cells through the release of exosomes. The findings of this research indicated that when the expression of *H19* suppressed, the resistance to Dox decreases by reducing cell viability and inducing apoptosis [30]. It has been found that *H19* has a role in the development of resistance to drugs in breast cancer through different mechanisms [31]. For instance, *H19* causes resistance to Dox through the regulation of the cullin4A-MDR1 signaling pathway [32].

Moreover, the results did not indicate that a specific lncRNA causes Dox resistance in all cancers. For instance, in BC cells, an oncogenic lncRNA *MALAT1* can significantly increase cell proliferation, migration, and

Dox resistance by targeting *miR-570-3p* [33]. However, in Hepatocellular Carcinoma (HCC), *LncARSR* induces Dox resistance via decreasing and activating of PTEN expression and PI3K pathway, respectively [34].

Another noteworthy point according to the studies mentioned in this article is that this expression change in lncRNAs can show itself in different cell groups such as cancer cells, CAFs, or even exosomes derived from them.

Our earlier research demonstrated that lncRNAs *H19* and *UCA1* were significantly upregulated in the BC sample [35]. Hence, our study found that serum exosomes of patients had a significantly higher-level expression of *H19* and *UCA1* ( $P < 0.0001$ ) compared to serum exosomes of normal women. Moreover, the current study revealed that CAFs had a significantly higher level of expressions of *H19* and *UCA1* compared to NFs ( $P < 0.0001$ ).

Studies have measured the expression of *H19* lncRNA in colorectal cancer-CAF [5] and oral cancer-CAF [36]. The level of expression of *H19* in BC-CAF cells was determined here for the first time and the upregulation among MDA-MB-231, MCF-7, and their co-culture with CAFs were confirmed.

Despite earlier studies suggesting that *H19* expression levels were correlated with tumor size, hormone receptor status (negatively), and lymph node status [37], our results did not support this. The difference might be due to factors such as the size and state of the investigated samples. Notably, every patient in this study had

a BC that was in stages one or two. Overall, the results highlighted the role of interaction between tumor cells and the surroundings in the development of BC. The interaction between CAFs and BC cells, as well as the role of exosomes and their cargo, may play a critical role in promoting the increase of drug resistance in breast cancer.

MSCs are recognized as a promising source of exosomes for clinical applications due to their unique abilities to regulate immunological functions, self-renewal, and tissue repair in a variety of disorders [38].

Researchers tend to use ultracentrifugation for exosome extraction, despite some disadvantages such as aggregation and fragmentation during exosome separation. However, polyethylene glycol (PEG) precipitation separation (which is used in exosome isolation kits) is another way to isolate MSC-Exos. According to [39], the yield of exosomes isolated with PEG was 14 times more than that of different centrifugation protocols.

In this study, exosome isolation from ADMSCs was performed using an exosome isolation kit. The amount of our MSC-Exos was 450  $\mu\text{g}/\mu\text{l}$ . MSCs-Exos can either promote or inhibit the growth of cancer cells and have comparable functional effects on MSCs [40]. The MTT assay results showed that the MSC-Exos had no noticeable effect on the cells, indicating that they might be a suitable drug delivery vehicle.

Sonication, a process involving the application of high-frequency sound waves to facilitate drug entry, stand as one of the most popular techniques for loading therapeutic compounds into exosomes [41]. Several studies have effectively utilized sonication to incorporate drugs such as 5-fluorouracil [42], curcumin, crocin [43], and Dox [44].

MSC- Exos sonicated and loaded with Dox were employed in this study to treat BC cells and CAFs. The results of TEM indicated that the Exo-Dox was successfully formed and maintained its structure, which could be a factor in the targeted delivery of Dox to cancer cells.

Research findings suggested that exosome-based therapies play a significant role in cancer treatments.

[45]. additionally, it was reported that exosomal curcumin had more antiproliferative efficacy in BC cell lines compared to free curcumin [46]. Exosomal paclitaxel demonstrated a pronounced reduction in the viability of BC cells [47]. These findings suggest that exosomes serve as appropriate nanocarriers for delivering a variety of molecular drugs.

As the results showed, the vitality of MDA-MB-231, MCF-7, MDA-MB-231, and MCF-7 cells co-cultured with CAFs decreased almost in a dose-dependent way. Based on the comparison of IC<sub>50</sub> of Dox shown in Table 2, it can be seen that this value is significantly higher for co-culture groups such as MCF-7 with CAF cells (5.3  $\mu\text{M}$ ) and MDA-MB-231 with CAF cells (no

IC<sub>50</sub>) compared to monoculture groups such as MCF-7 (2.3  $\mu\text{M}$ ) and MDA-MB-231 (5.1  $\mu\text{M}$ ). This, confirms that when CAF cells are present, the drug resistance is much higher and as a result, a higher dose of Dox is needed.

In spite of Exo-Dox-induced apoptosis, Dox-induced apoptosis was not observed noticeably in a co-culture of MDA-MB-231 cells and CAFs. This indicates that Exo-Dox has a higher ability to kill cancer cells. Since exosomes may enter cells through endocytosis, micropinocytosis, and phagocytosis [48], the Exo-Dox sustains less damage compared to the free Dox. Therefore, Exo-Dox is more successful in killing cancer cells [49]. Moreover, comparing the survival rates of normal fibroblast cells treated with equal concentrations such as 5 and 10 micromolar Dox (Fig. 4B) and Exo-Dox (Fig. 4H) over a 48 h period, it becomes evident that the toxicity of Exo-Dox was significantly higher than doxorubicin ( $p < 0.05$ ).

The morphological observation analysis in live and dead assays showed that the cells treated with Exo-Dox displayed apoptotic characteristics. Hence, Exo-Dox was significantly internalized by MDA-MB-231 and co-culture of MDA-MB-231 with CAF cells and leading to cell death.

Comparison of the antitumor effect between Exo-Dox and Dox in animal studies showed that Exo-Dox has a greater effect. Our study revealed that the in vivo results were completely in agreement with the results of in vitro results.

Overall, our findings indicated that the expression levels of *H19* and *UCA1* in exosome-derived CAFs were significantly higher in BC patients, and their strong identification abilities suggested their potential as candidate biomarkers for BC diagnosis and treatment. Additionally, the elevated expression levels of the *TP53* gene in MDA-MB-231 and the co-culture of MDA-MB-231 with CAFs treated groups suggested its potential as a therapeutic target for BC.

## Conclusion

Exo-Dox was created using the sonication process with a 59% entrapment efficiency. Exo-Dox had a lower IC<sub>50</sub> value than free Dox in the aggressive MDA-MB-231 cells and MDAMB-231 co-cultured with CAFs. Exo-Dox treated cells demonstrated dramatically decreased levels of *H19* and *UCA1* expression with considerably increased levels of *TP53* expression. Moreover, Exo-Dox showed remarkable anti-tumor efficacy in Tumor-bearing mice. Thus, we conclude that exosomes can be employed to deliver Dox to cancer cells, especially in tumors resistant to treatment. Exo-Dox treatment could be a desirable strategy to regulate lncRNA expression in BC cells and target CAFs. However, more research work is required to fully understand the processes behind Exo-Dox's effects on CAFs and BC cells.

## Supplementary Information

The online version contains supplementary material available at <https://doi.org/10.1186/s12935-025-03689-y>.

Supplementary Material 1

### Author contributions

FAA performed the experiments, contributions to the conception, the acquisition, analysis and wrote the first draft of the manuscript; SI designed the study; SI and MO supervision and all data curation; AB, LG, and FA analyzed data. All authors read and approved the final manuscript.

### Funding

This research did not receive any funding.

### Data availability

No datasets were generated or analysed during the current study.

### Declarations

### Ethical approval

The study was carried out based on the approval by the Ethics Committee of the Science and Research Branch, Islamic Azad University of Medical Sciences, under the permission code IR.IAU.SRB.REC.1401.362. An informed consent letter was signed by all the participants and the ethical committee of the Islamic Azad University (Approval number: IR.IAU.SRB.REC.1401.362) approved the study. The experiments on animals was in accordance with the ARRIVE guidelines.

### Competing interests

The authors declare no competing interests.

Received: 22 September 2024 / Accepted: 12 February 2025

Published online: 27 February 2025

### References

- Piombino C, Mastrolia I, Omarini C, Candini O, Dominici M, Piacentini F, Toss A. The role of exosomes in breast cancer diagnosis. *Biomedicines*. 2021. <https://doi.org/10.3390/biomedicines9030312>.
- Truffi M, Sitia L, Sevieri M, Bonizzi A, Rizzuto MA, Mazzucchelli S, Corsi F. Isolation of primary cancer-associated fibroblasts from a syngeneic murine model of breast cancer for the study of targeted nanoparticles. *J Visualized Experiments*. 2021. <https://doi.org/10.3791/62504>.
- Barth DA, Juracek J, Slaby O, Pichler M, Calin GA. lncRNA and mechanisms of drug resistance in cancers of the genitourinary system. *Cancers*. 2020. <https://doi.org/10.3390/cancers12082148>.
- Ti W, Wang J, Cheng Y. The interaction between long non-coding RNAs and cancer-associated fibroblasts in lung cancer. *Front Cell Dev Biology*. 2022. <https://doi.org/10.3389/fcell.2021.714125>.
- Ren J, Ding L, Zhang D, Shi G, Xu Q, Shen S, Wang Y, Wang T, Hou Y. Carcinoma-associated fibroblasts promote the stemness and chemoresistance of colorectal cancer by transferring exosomal lncRNA H19. *Theranostics*. 2018. <https://doi.org/10.7150/thno.25541>.
- Gao Q, Fang X, Chen Y, Li Z, Wang M. Exosomal lncRNA UCA1 from cancer-associated fibroblasts enhances chemoresistance in vulvar squamous cell carcinoma cells. *J Obstet Gynecol Res*. 2021. <https://doi.org/10.1111/jog.14418>.
- Sharifi S, Barar J, Hejazi MS, Samadi N. Doxorubicin changes Bax/Bcl-xL ratio, caspase-8 and 9 in breast cancer cells. *Adv Pharm Bull*. 2015. <https://doi.org/10.15171/apb.2015.049>.
- Mobaraki M, Faraji A, Zare M, Dolati P, Ateai M, Manshadi HD. Molecular mechanisms of cardiotoxicity: a review on major side-effect of doxorubicin. *Indian J Pharm Sci*. 2017. <https://doi.org/10.4172/pharmaceutical-sciences.1000235>.
- Ferrari M. Cancer nanotechnology: opportunities and challenges. *Nat Rev Cancer*. 2005. <https://doi.org/10.1038/nrc1566>.
- Couvreur P, Vauthier C. Nanotechnology: intelligent design to treat complex disease. *Pharm Res*. 2006. <https://doi.org/10.1007/s11095-006-0284-8>.
- Salarpour S, Forooutfar H, Pournamdari M, Ahmadi-Zeidabadi M, Esmaeeli M, Pardakhty A. Paclitaxel incorporated exosomes derived from glioblastoma cells: comparative study of two loading techniques. *DARU J Pharm Sci*. 2019. <https://doi.org/10.1007/s40199-019-00280-5>.
- Urbanelli L, Magini A, Buratta S, Brozzi A, Sagini K, Polchi A, Tancini B, Emiliani C. Signaling pathways in exosomes biogenesis, secretion and fate. *Genes*. 2013. <https://doi.org/10.3390/genes4020152>.
- Escrevente C, Keller S, Altevogt P, Costa J. Interaction and uptake of exosomes by ovarian cancer cells. *BMC Cancer*. 2011. <https://doi.org/10.1186/1471-2407-11-108>.
- Bell BM, Kirk ID, Hiltbrunner S, Gabriellson S, Bultema JJ. Designer exosomes as next-generation cancer immunotherapy. *Nanomater Nanotechnol Biol Med*. 2016. <https://doi.org/10.1016/j.nano.2015.09.011>.
- Lee JK, Park SR, Jung BK, Jeon YK, Lee YS, Kim MK, Kim YG, Jang JY, Kim CW. Exosomes derived from mesenchymal stem cells suppress angiogenesis by down-regulating VEGF expression in breast cancer cells. *PLoS ONE*. 2013. <http://doi.org/10.1371/journal.pone.0084256>.
- Toffoli G, Hadla M, Corona G, Caligiuri I, Palazzolo S, Semeraro S, Gamini A, Canzonieri V, Rizzolio F. Exosomal doxorubicin reduces the cardiac toxicity of doxorubicin. *Nanomedicine*. 2015. <https://doi.org/10.2217/nnm.15.118>.
- Raguraman R, Bhavsar D, Kim D, Ren X, Sikavitsas V, Munshi A, Ramesh R. Tumor-targeted exosomes for delivery of anticancer drugs. *Cancer Lett*. 2023. <https://doi.org/10.1016/j.canlet.2023.216093>.
- Kumar P, Aggarwal R. An overview of triple-negative breast cancer. *Arch Gynecol Obstet*. 2016. <https://doi.org/10.1007/s00404-015-3859-y>.
- Al-Mahmood S, Sapiezynski J, Garbuzenko OB, Minko T. Metastatic and triple-negative breast cancer: challenges and treatment options. *Drug Delivery Translational Res*. 2018. <https://doi.org/10.1007/s13346-018-0551-3>.
- Chen X, Song E. Turning foes to friends: targeting cancer-associated fibroblasts. *Nat Rev Drug Discovery*. 2019. <https://doi.org/10.1038/s41573-018-0004-1>.
- Fernández-Nogueira P, Fuster G, Gutierrez-Uzquiza Á, Gascón P, Carbó N, Bragado P. Cancer-associated fibroblasts in breast cancer treatment response and metastasis. *Cancers*. 2021. <https://doi.org/10.3390/cancers13133146>.
- Wen S, Hou Y, Fu L, Xi L, Yang D, Zhao M, Qin Y, Sun K, Teng Y, Liu M. Cancer-associated fibroblast (CAF)-derived IL32 promotes breast cancer cell invasion and metastasis via integrin  $\beta 3$ -p38 MAPK signalling. *Cancer Lett*. 2019. <https://doi.org/10.1016/j.canlet.2018.10.015>.
- Bermúdez M, Aguilar-Medina M, Lizárraga-Verdugo E, Avendaño-Félix M, Silva-Benítez E, López-Camarillo C, Ramos-Payán R. lncRNAs as regulators of autophagy and drug resistance in colorectal cancer. *Front Oncol*. 2019. <https://doi.org/10.3389/fonc.2019.01008>.
- Du T, Shi Y, Xu S, Wan X, Sun H, Liu B. Long non-coding RNAs in drug resistance of breast cancer. *Oncotargets Therapy*. 2020. <https://doi.org/10.2147/OTT.S255226>.
- Lakshmi S, Hughes TA, Priya S. Exosomes and exosomal RNAs in breast cancer: a status update. *Eur J Cancer*. 2021. <https://doi.org/10.1016/j.ejca.2020.11.033>.
- Jia Y, Chen Y, Wang Q, Jayasinghe U, Luo X, Wei Q, Wang J, Xiong H, Chen C, Xu B, Hu W. Exosome: emerging biomarker in breast cancer. *Oncotarget*. 2017. <https://doi.org/10.18632/oncotarget.16684>.
- Hu D, Li Z, Zheng B, Lin X, Pan Y, Gong P, Zhuo W, Hu Y, Chen C, Chen L, Zhou J. Cancer-associated fibroblasts in breast cancer: challenges and opportunities. *Cancer Commun*. 2022. <https://doi.org/10.1002/cac2.12291>.
- Sansone P, Savini C, Kurelac I, Chang Q, Amato B L, Strillacci A, Stepanova A, Iommarini L, Mastroleo C, Daly L, Galkin A. Packaging and transfer of mitochondrial DNA via exosomes regulate escape from dormancy in hormonal therapy-resistant breast cancer. *Proc Natl Acad Sci*. 2017. <https://doi.org/10.1073/pnas.1704862114>.
- Xu CG, Yang MF, Ren YQ, Wu CH, Wang LQ. Exosomes mediated transfer of lncRNA UCA1 results in increased tamoxifen resistance in breast cancer cells. *Eur Rev Med Pharmacol Sci*. 2016;20:20.
- Wang X, Pei X, Guo G, Qian X, Dou D, Zhang Z, Xu X, Duan X. Exosome-mediated transfer of long noncoding RNA H19 induces doxorubicin resistance in breast cancer. *J Cell Physiol*. 2020. <https://doi.org/10.1002/jcp.29585>.
- Collette J, Le Bourhis X, Adriaenssens E. Regulation of human breast cancer by the long non-coding RNA H19. *Int J Mol Sci*. 2017. <https://doi.org/10.3390/ijms18112319>.
- Zhu QN, Wang G, Guo Y, Peng Y, Zhang R, Deng JL, Li ZX, Zhu YS. lncRNA H19 is a major mediator of doxorubicin chemoresistance in breast cancer cells

- through a cullin4A-MDR1 pathway. *Oncotarget*. 2017. <https://doi.org/10.18632/oncotarget.21121>.
33. Yue X, Wu WY, Dong M, Guo M. LncRNA MALAT1 promotes breast cancer progression and doxorubicin resistance via regulating miR-570-3p. *Biomedical J*. 2021. <https://doi.org/10.1016/j.bj.2020.11.002>.
  34. Li Y, Li J, Chen H, Wang J, Jiang L, Tan X. The lncARSR/PTEN/Akt/nuclear factor-kappa B feedback regulatory loop contributes to doxorubicin resistance in hepatocellular carcinoma. *J Biochem Mol Toxicol*. 2022. <https://doi.org/10.1002/jbt.23119>.
  35. Pourramezan Z, Attar FA, Yusefpour M, Azizi M, Oloomi M. Circulating LncRNAs landscape as potential biomarkers in breast cancer. *Cancer Rep*. 2023. <https://doi.org/10.1002/cnr2.1722>; <https://doi.org/10.1161/CIRCRESAHA.114.303915>
  36. Yang J, Shi X, Yang M, Luo J, Gao Q, Wang X, Wu Y, Tian Y, Wu F, Zhou H. Glycolysis reprogramming in cancer-associated fibroblasts promotes the growth of oral cancer through the lncRNA H19/miR-675-5p/PFKFB3 signaling pathway. *Int J Oral Sci*. 2021. <https://doi.org/10.1038/s41368-021-00115-7>.
  37. Shima H, Kida K, Adachi S, Yamada A, Sugae S, Narui K, Miyagi Y, Nishi M, Ryo A, Murata S, Taniguchi H. Lnc RNA H19 is associated with poor prognosis in breast cancer patients and promotes cancer stemness. *Breast Cancer Res Treat*. 2018. <https://doi.org/10.1007/s10549-018-4793-z>.
  38. Naseri Z, Oskuee RK, Forouzandeh-Moghadam M, Jaafari MR. Delivery of LNA-anti-miR-142-3p by mesenchymal stem cells-derived exosomes to breast cancer stem cells reduces tumorigenicity. *Stem Cell Reviews Rep*. 2020. <https://doi.org/10.1007/s12015-019-09944-w>.
  39. Börger V, Staubach S, Dittrich R, Stambouli O, Giebel B. Scaled isolation of mesenchymal stem/stromal cell-derived extracellular vesicles. *Curr Protoc Stem Cell Biol*. 2020. <https://doi.org/10.1002/cpsc.128>.
  40. Damala M, Kethiri AR, Tavakkoli F, Raju E, Singh V. The basics of stem cells and their role in vision. *Trends Life Sci Res*. 2018;97:123.
  41. Kibria G, Ramos EK, Wan Y, Gius DR, Liu H. Exosomes as a drug delivery system in cancer therapy: potential and challenges. *Mol Pharm*. 2018. <https://doi.org/10.1021/acs.molpharmaceut.8b00277>.
  42. Chen M, Li Y, Ma N, Zang J. Mesenchymal stem cell-derived exosomes loaded with 5Fu against cholangiocarcinoma in vitro. *Mol Med Rep*. 2022. <https://doi.org/10.3892/mmr.2022.12729>.
  43. Abbasifarid E, Bolhassani A, Irani S, Sotoodehnejadmatalahi F. Synergistic effects of exosomal crocin or curcumin compounds and HPV L1-E7 polypeptide vaccine construct on tumor eradication in C57BL/6 mouse model. *PLoS ONE*. 2021. <https://doi.org/10.1371/journal.pone.0258599>.
  44. Xie X, Lian S, Zhou Y, Li B, Lu Y, Yeung I, Jia L. Tumor-derived exosomes can specifically prevent cancer metastatic organotropism. *J Controlled Release*. 2021. <https://doi.org/10.1016/j.jconrel.2021.01.030>.
  45. Bai Y, Guo J, Liu Z, Li Y, Jin S, Wang T. The role of exosomes in the female reproductive system and breast cancers. *OncoTargets Therapy*. 2020. <https://doi.org/10.2147/OTT.S281909>.
  46. Aqil F, Munagala R, Jeyabalan J, Agrawal AK, Gupta R. Exosomes for the enhanced tissue bioavailability and efficacy of curcumin. *AAPS J*. 2017. <https://doi.org/10.1208/s12248-017-0154-9>.
  47. Kalimuthu S, Gangadaran P, Rajendran RL, Zhu L, Oh JM, Lee HW, Gopal A, Baek SH, Jeong SY, Lee SW, Lee J. A new approach for loading anticancer drugs into mesenchymal stem cell-derived exosome mimetics for cancer therapy. *Front Pharmacol*. 2018. <https://doi.org/10.3389/fphar.2018.01116>.
  48. Mulcahy LA, Pink RC, Carter DR. Routes and mechanisms of extracellular vesicle uptake. *J Extracell Vesicles*. 2014. <https://doi.org/10.3402/jev.v3.24641>.
  49. Chowdhury N, Chaudhry S, Hall N, Olverson G, Zhang QJ, Mandal T, Dash S, Kundu A. Targeted delivery of doxorubicin liposomes for Her-2 + breast cancer treatment. *AAPS PharmSciTech*. 2020. <https://doi.org/10.1208/s12249-020-01743-8>.

#### Publisher's note

Springer Nature remains neutral with regard to jurisdictional claims in published maps and institutional affiliations.